

# Preparation, Microstructure and Thermal Property of $\text{ZrAl}_3/\text{Al}$ Composite Fuels

Aobo Hu,<sup>[a]</sup> Hui Zou,<sup>[a]</sup> Wen Shi,<sup>[a]</sup> Ai-min Pang,<sup>\*,[b]</sup> and Shuizhou Cai<sup>\*,[a]</sup>

**Abstract:**  $\text{ZrAl}_3/\text{Al}$  composite fuels ( $\text{Al-xZr}$ ,  $x = 10, 20, 30, 40, 50, 53$  wt.%) were prepared by the non-consumable arc-melting technique and close-coupled gas-atomization. In order to study the effects of the zirconium content and the oxygen partial pressure on the thermal properties of composite fuels, X-ray diffraction, scanning electron microscopy, TG-DTA and DSC were used to characterize the composite fuels, respectively. The result shows that the addition of zirconium leads to the formation of a special structure inside the powder, promoting the oxidation of  $\text{ZrAl}_3/\text{Al}$  composite fuels. Besides, non-selective oxidation of  $\text{ZrAl}_3$  played an important role in promoting the oxidation process. The oxygen bomb experiment was conducted to evaluate the combustion performance of  $\text{ZrAl}_3/\text{Al}$  composite fuels. Oxygen bomb experiments show that the gravimetric

combustion enthalpy of the composite fuels decreases linearly with the increase of zirconium content, and increases with the increase of oxygen partial pressure. However, the volumetric combustion enthalpy decreases first and then increases with the increase of zirconium content, and shows a general upward trend when the partial pressure of oxygen reaches 2.5 MPa or more. The pressure curve indicates that the  $\text{Al-53Zr}$  composite fuels have the maximum pressure propagation rate  $(dP/dt)_{\max}$  (which characterizes the maximum flame propagation rate and higher energy releasing rates) in the prepared series of composite fuels. The study demonstrates a complete combustion of  $\text{ZrAl}_3/\text{Al}$  composite fuels under high pressure.  $\text{ZrAl}_3/\text{Al}$  composite fuels could be considered as a very promising energetic additive in the field of new-energetic material.

**Keywords:**  $\text{ZrAl}_3/\text{Al}$  composite fuels · Intermetallic compounds · Oxidation properties · Combustion characteristic · Density

## 1 Introduction

Metal fuels, as high-energy additives and combustion catalysts filling in the propellant and explosive to improve density, detonation heat and specific impulse of engine, have been widely employed in research and development for the improvement of aerospace and weapon systems [1–3]. Currently, the studies on metal fuels mainly focus on aluminum and Al-based alloy powders, such as Al–Mg, Al–Li, Al–Ni, Al–Ti, and so on [4–7]. To some degree, the alloy powders mentioned above can shorten the ignition delay time, reduce the ignition temperature and strengthen the degree of oxidation. They also have higher energy releasing efficiency and energy releasing rates [8–10]. However, these metals have some essential shortcomings. For example, Al powder has the defects of agglomeration and incomplete combustion [11–15], Mg has the drawback of low air/fuel ratio for ramjet application [16].


Zirconium is one of the representative energetic materials with high density. The higher density can lead to higher volumetric impulse and higher energy density [16–18]. In addition, the good ignition performance is also one of the reasons for the enduring interest in research of zirconium [19,20]. This property makes it easy to ignite even at higher loading. Zirconium is therefore emerging as a potential component of metallized propellants and other energetic formulations. However, the fundamental flaws of zirconium

powders, such as lower energy density than aluminum, and the high melting point (1852 °C), have limited the application and development of zirconium. Further, the zirconium powder is not sufficiently burned in the air, a large amount of unburned metal remains in the combustion products [21,22]. Thus, it is significant to develop  $\text{ZrAl}_3/\text{Al}$  composite fuels.

Nowadays, Al–Zr alloys are mainly prepared by self-propagating high-temperature synthesis (SHS) and non-consumable arc-melting technique [23–27]. SHS, a relatively new and promising method for synthesis of some simple intermetallic compounds, mainly relies on the highly exothermic reactions among the raw materials. Song et al. [23] used SHS reaction to fabricate the  $\text{ZrAl}_3$  intermetallic com-

[a] A. Hu, H. Zou, W. Shi, S. Cai  
State Key Laboratory of Material Processing and Die & Mould Technology, The School of Materials Science and Engineering  
Huazhong University of Science and Technology, Wuhan 430074, PR China  
\*e-mail: szcai@hust.edu.cn

[b] A.-m. Pang  
Science and Technology on Aerospace Chemical Power Laboratory  
Hubei Institute of Aerospace Chemotechnology, Xiangyang 441003, PR China  
\*e-mail: ppam@tom.com

 Supporting information for this article is available on the WWW under <https://doi.org/10.1002/prep.201900012>

pound by using starting powders consisted of aluminum and zirconium, these powders with the atomic ratio of Zr:Al = 1:3 were thoroughly mixed by ball milling and then were pressed into a green compact in advance. Non-consumable arc-melting technique has been widely used in melting of metals with high melting point and refractory. Paljevic [26,27] chose the stoichiometric amounts of Zr and Al ingots to melt together by using non-consumable arc-melting technique in a water-cooled copper mould under argon to prepare the ZrAl<sub>2</sub> and ZrAl<sub>3</sub>, respectively. Nevertheless, the materials prepared by both methods are bulk metals, and the microstructures of materials presented irregular morphologies. These disadvantages greatly affect the properties of materials and are not conducive to the application of materials in the field of propellants and explosives. In addition, the Weihs group fabricated the reactive Al/Zr multilayer foils by DC magnetron sputtering [28,29]. Recently, they have also synthesized a variety of Al–Zr alloys and composite powders by ball milling and physical vapor deposition (PVD) and tested them in various ignition and combustion experiments [30,31]. However, the powders prepared by these methods have a low degree of sphericity. In order to prepare the highly spherical ZrAl<sub>3</sub>/Al composite powder, a new technology is proposed.

This paper is aimed at preparing the ZrAl<sub>3</sub>/Al composite fuels by combining the non-consumable arc-melting technique with a close-coupled gas-atomization (CCGA). The composite fuels prepared by this method solve the problems of the currently applied pure aluminum fuel, such as incomplete combustion, high exothermic temperature. At the same time, the density of the fuels is increased. The microstructure and thermal properties of ZrAl<sub>3</sub>/Al composite fuels were thoroughly investigated.

## 2 Experimental Section

### 2.1 Preparation of ZrAl<sub>3</sub>/Al Composite Fuels

The Al<sub>3</sub>Zr/Al composite fuels with different Zr content were prepared by the following process. Appropriate amounts of zirconium sponge (purity, 99.99%) and aluminum ingots (purity, 99.95%) at fixed proportion were melted together using a non-consumable arc-melting technique in a water-cooled copper mould to produce the Al–Zr alloy ingots. Before melting, the sample chamber of the smelting furnace was pumped into a high vacuum state (vacuum  $\leq 4 \times 10^{-3}$  Pa), then argon as protection atmosphere was bubbled through the sample chamber until atmospheric pressure was reached. The residual oxygen in the sample chamber was absorbed three times by the molten titanium ball. Then the raw materials with different content of zirconium were melted together to prepare the Al–xZr alloy (x = 10, 20, 30, 40, 50, 53 wt.%). The current was adjusted as per different Zr content. The prepared alloys were generally melted about eight times to ensure homogeneity. A close-coupled

gas-atomization (CCGA) instrument was the main equipment for preparing Al–xZr composite fuels [32–34]. The obtained Al–Zr mother alloys were atomized in the CCGA equipment. The atomization conditions were as follows: the atomizing gas was pure argon, the spray gas pressure was 5 MPa, the maximum heating temperature was 1500 °C and the vacuum degree was 20 Pa. And above all, temperature and pressure were key parameters. Atomization may fail if these parameters are not controlled well. After the atomization process, the obtained powders were sieved by a 200-mesh sieve.

### 2.2 Characterization of Materials

The morphology of the powders was characterized using a scanning electron microscope (Nova Nano SEM 450) coupled with an energy-dispersive X-ray spectrometer (EDS). Backscattered electron images were applied to observe particle shapes and sizes. Appropriate samples were embedded in epoxy resin, ground and polished, then corroded by corrosion solution with the volume ratio of HF:HCl:HNO<sub>3</sub>:H<sub>2</sub>O = 1:1.5:2.5:95. The obtained samples were used for particle cross-section analysis.

Phase compositions of the powders were characterized by means of X-ray diffractometer (Empyrean) with Cu K $\alpha$  radiation, and the patterns were collected in the angular range 10°–90° in 2 $\theta$ . The furnace-cooling oxidation products and combustion products were collected and analyzed.

The thermal analysis experiments were carried out on a Diamond TG/DTA, made by PerkinElmer Instruments, from room temperature to 1300 °C in an O<sub>2</sub> atmosphere with gas flowing at 20 mL/min and at a heating rate of 20 °C/min. The differential scanning calorimetry (DSC) test was performed on a Diamond DSC, made by PerkinElmer Instruments. Samples were heated in argon and oxygen atmosphere, respectively, ranging from room temperature to 1000 °C with gas flowing at 20 mL/min and at a heating rate of 10 °C/min.

A spring dynamometer method was used to determine densities of the produced Al–Zr alloys. In this paper, bulk density of alloys was substituted for the stacking density of powders. The bulk densities of alloys obtained based on the formula (1) and (2) is as follows. All coefficients and variables are defined in a list after the text.

$$F = G - T_0 = \rho_0 g V_0 \quad (1)$$

### 2.3 Oxygen Bomb Calorimeter

A full automatic calorimeter based on microcomputer control system with touch-sensitive screens (ZDHW-8Z, Hebi Keda Instrument and Meter Co., Ltd, R. P. China), is used to measure the combustion enthalpy of composite fuels. The

schematic diagram of the experimental device is shown in Figure 1. The improved calorimeter meets the design re-

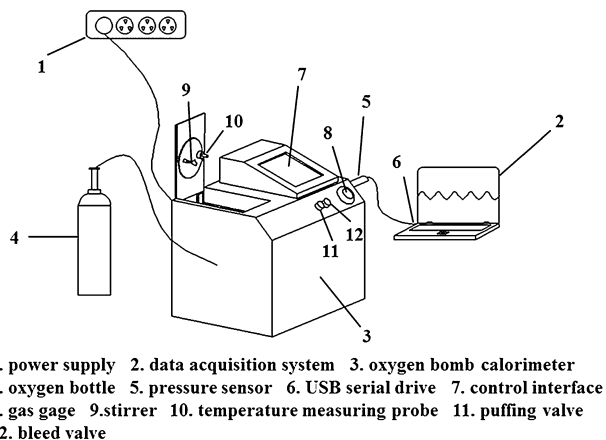


**Figure 1.** The schematic diagram of the oxygen bomb calorimeter apparatus.

quirements and can provide a reference for solving the same types of problems. The sample holder which is made of tungsten has excellent heat-resistance. Compared with the general calorimeter, the improved calorimeter has new functions. Pressure change in the oxygen bomb before and after the ignition of the sample can be monitored synchronously by a pressure sensor that connects to the data acquisition system. The information can be displayed in the form of visual image directly. The experimental principle of the device is similar to the experiment principle reported in [35]. Different  $\text{ZrAl}_3/\text{Al}$  composite fuels were tested at different pressures in the device shown in Figure 1. To prevent mass transfer effects, all samples should be weighed with equal precision (0.15 grams) with a high-precision electronic balance. Then combustion enthalpy and pressure variation curves were recorded.

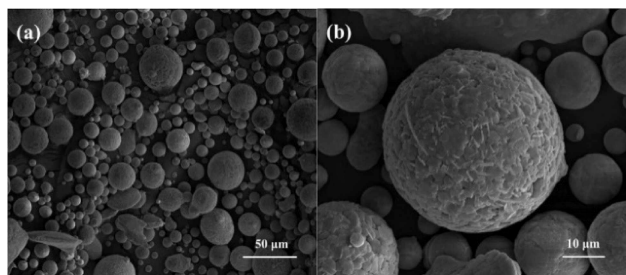


**Figure 2.** SEM images of Al-30Zr composite fuels.

### 3 Results and Discussion

#### 3.1 Powder Morphology, Microstructure and Phase Composition

Figure 2 shows the SEM micrographs of the Al-30Zr composite fuels prepared by the CCGA. As shown in Figure 2(a), most powder materials are highly spherical and there is no significant agglomeration. Figure 2(b) displays the surface morphology of individual particle. It can be observed that the surface of the particle is very rough. Apparent grain boundaries can be observed on the surface of the particles. It seems like some scales deposited on the surface. The formation of scales is due to the existence of oriented crystal-line surfaces and crystallographic direction during solidification process. There is one phase in the particle that has preferential orientation and preferential crystallization.

Figure 3 displays the SEM and EDS spectra of the cross section of the composite fuels. As can be clearly seen from the diagram, the white acicular crystals are embedded in the black matrix. The white needle-shaped crystals take the role of grain refinement. The EDS analysis indicates that the content of zirconium distributed in the white acicular crystals is as high as 25.34 at.% and the content of aluminum is 74.66 at.%. This result suggests that intermetallic reactions between aluminum and zirconium occur during the process of forming intermetallic compounds by CCGA. Therefore, the white acicular phase observed should be  $\text{ZrAl}_3$ . While the content of aluminum distributed in the black matrix reaches 96.82 at.%, the zirconium content is almost negligible. Therefore, the black phase is Al. This result is consistent with the results of XRD shown in Figure 4, which reveals that there are two phases, namely,  $\text{ZrAl}_3$  and excess Al presented in the particle. The needle-shaped intermetallic compounds are embedded in the aluminum matrix, separating the aluminum in the matrix. Thus, a unique structure is found in the interior of the composite powder. It is believed that this particular structure may plays a major role in facilitation for oxidation of particle.

XRD patterns showing the phase transformation and relative content evolution of the  $\text{ZrAl}_3/\text{Al}$  composite fuels with different zirconium concentrations are exhibited in Figure 4. The result shows that only Al and  $\text{ZrAl}_3$  are found in the  $\text{ZrAl}_3/\text{Al}$  composite fuels, which are consistent with the Al–Zr phase diagram. There is no characteristic peak of Zr on the XRD patterns, which indicates that Zr has been totally alloyed with Al to form the intermetallic compound  $\text{ZrAl}_3$ . Furthermore, the XRD result also shows that  $\text{ZrAl}_3$  peaks become stronger with the increasing content of zirconium. When the content of zirconium increases to 53 wt.% (The corresponding atom fraction is 25 at.%), all of the phases are transformed into  $\text{ZrAl}_3$ , and Al peaks are completely absent from the diffraction patterns.

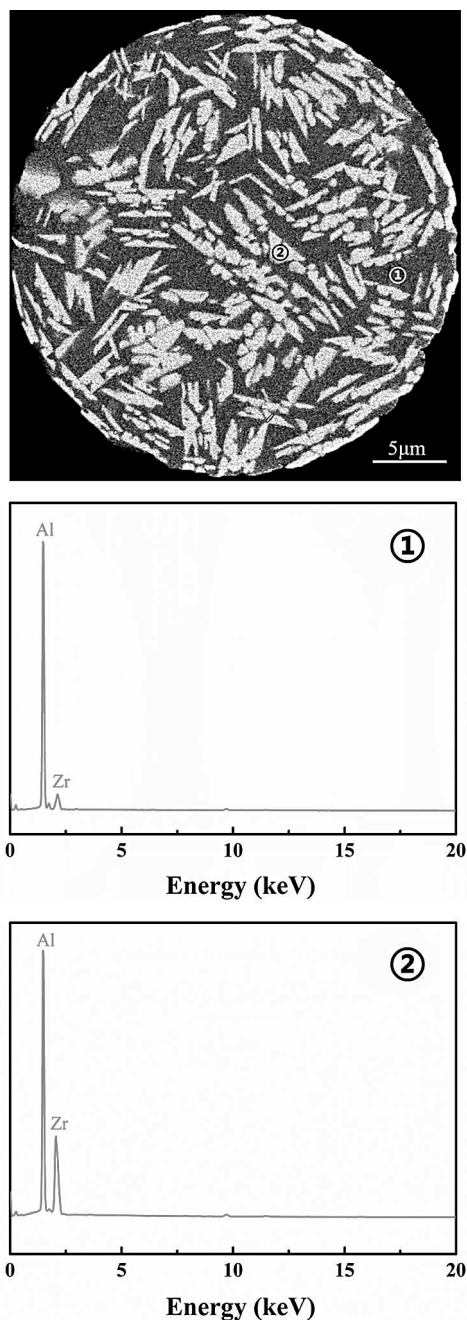


**Figure 3.** SEM image and EDS elemental spectrums of the particle cross-section of the Al-30Zr composite fuels.

### 3.2 Thermal Analysis

Figure 5 shows the TG-DTA curves of the  $\text{ZrAl}_3/\text{Al}$  composite fuels with different zirconium content. As can be seen from the Figure 5(a), there is an endothermic peak caused by the melting of aluminum occurs at about  $660^\circ\text{C}$  with Zr content ranging from 10 wt.% to 40 wt.%, followed by a relatively obvious exothermic peak. Apparently, when the content of zirconium exceeds 40 wt.%, since a majority of alu-

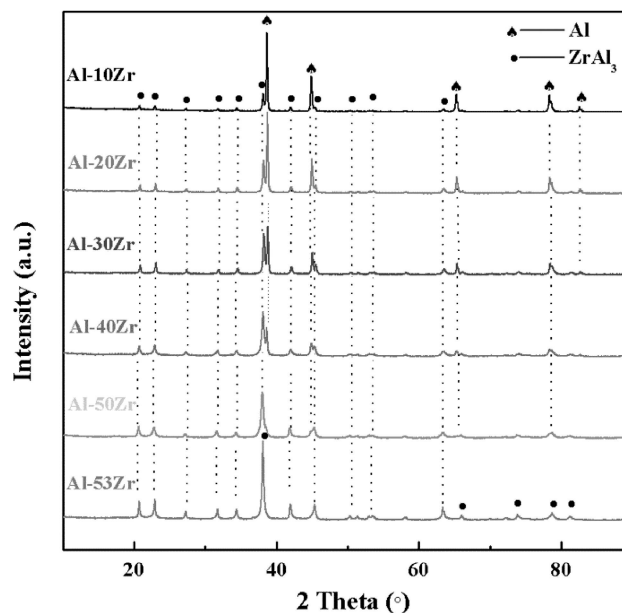


**Figure 4.** XRD patterns of  $\text{ZrAl}_3/\text{Al}$  composite fuels.

minum and zirconium have been transformed into the  $\text{ZrAl}_3$ , the endothermic peak of aluminum begins to become less pronounced, but the exothermic peak of the composite fuels gets more significant. Meanwhile the exothermic peak of the composite fuels with the Zr content of less than 40 wt.% appear at about  $1000^\circ\text{C}$ . When the Zr content reaches 50 wt.% and 53 wt.%, a sharp exothermic peak appears at about  $960^\circ\text{C}$ . Figure 5(b) shows the TG curves of the  $\text{ZrAl}_3/\text{Al}$  composite fuels. As illustrated in Figure 5(b), with the increasing content of zirconium, The weight increase ratio of  $\text{ZrAl}_3/\text{Al}$  composite powder is quite apparent, which all is more than that of pure Al reported in previous studies [32]. However, when the zirconium content is less than or equal to 30 wt.%, the weight increase ratio of the composite fuels is not much different, and when the zirconium content reaches 40 wt.% or more, the weight increase ratio of the composite fuels suddenly significantly increases. In addition, in combination with the results in the DTA curves, it is observed that the temperature required to achieve the maximum weight gain efficiency is significantly reduced with the increasing content of zirconium. We suspect that the reason is related to the  $\text{ZrAl}_3$  in the  $\text{ZrAl}_3/\text{Al}$  composite fuels.

In order to study how the  $\text{ZrAl}_3$  in composite powder affects the thermal analysis results, the pure intermetallic compound  $\text{ZrAl}_3$  powders (the Al-53Zr alloy powders) were exposed to the oxygen and heated to  $600^\circ\text{C}$ ,  $800^\circ\text{C}$ ,  $900^\circ\text{C}$  and  $1000^\circ\text{C}$ , respectively. Figure 6 shows the XRD patterns of  $\text{ZrAl}_3$  oxidation products at every temperatures. As can be seen from the Figure 6,  $\text{ZrAl}_3$  is basically not subjected to oxidation at  $600^\circ\text{C}$ . As the oxidation temperature increases from  $600^\circ\text{C}$  to  $800^\circ\text{C}$ ,  $\text{ZrAl}_3$  peaks disappear from the XRD patterns, which are replaced by  $\text{Al}_2\text{O}_3$ , t- $\text{ZrO}_2$  and m- $\text{ZrO}_2$ .

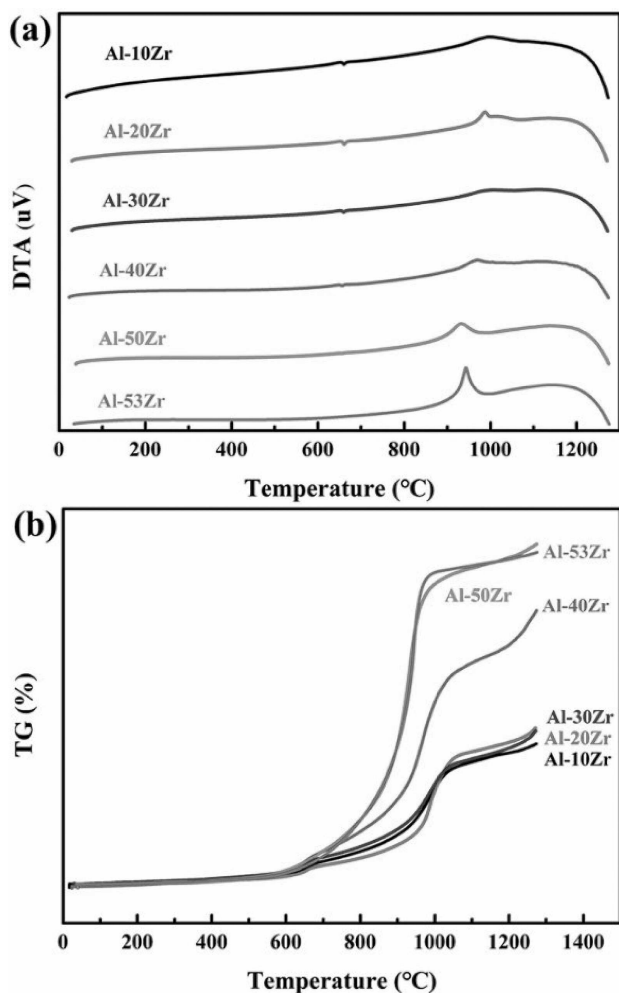


Figure 5. TG-DTA curves of  $\text{ZrAl}_3/\text{Al}$  composite fuels with different Zr contents.

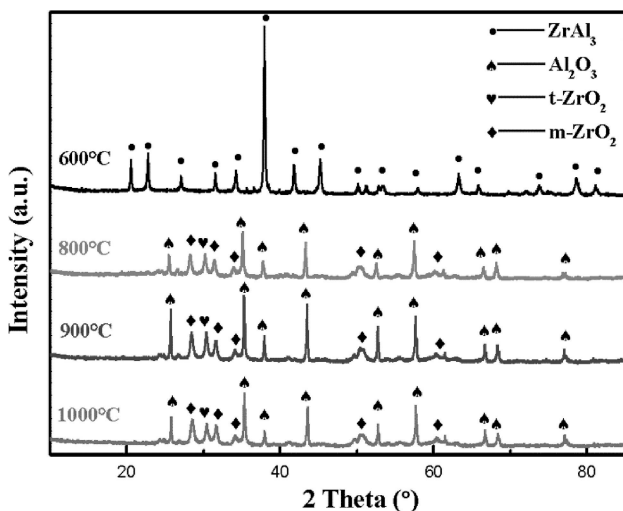


Figure 6. XRD patterns of the  $\text{ZrAl}_3$  oxidation products at different temperatures.

The peak positions do not change but the relative intensities change when the temperature reaches both 900°C and 1000°C. This indicates the  $\text{ZrAl}_3$  is not completely oxidized at 800°C and further oxidation occurs when the temperature exceeds 800°C. However, the compositions of the products do not change and there is no obvious crystalline transition at 960°C. Based on the above description and discussion, it is inferred that there is no correlation between the crystalline transition of the oxidation products and the exothermic reaction at 960°C during the oxidation process of the  $\text{ZrAl}_3/\text{Al}$  composite fuels.

Subsequently, in order to confirm whether pure  $\text{ZrAl}_3$  has a heat release near 960°C, DSC experiments were carried out respectively in argon gas and oxygen ambience with the temperature range of 20–1000°C. As shown in Figure 7, the result of DSC indicates that there is no obvious

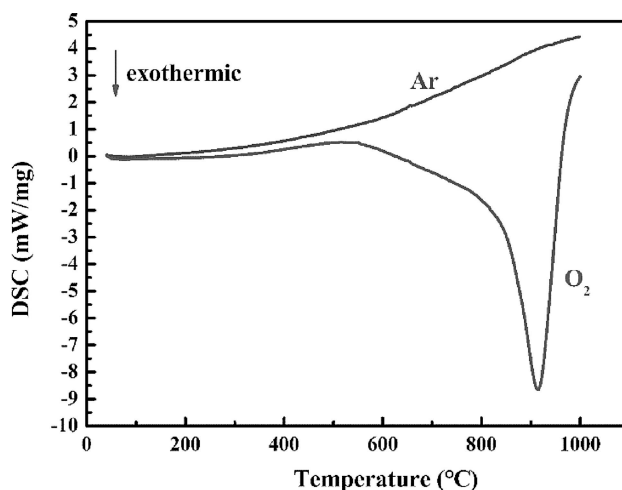
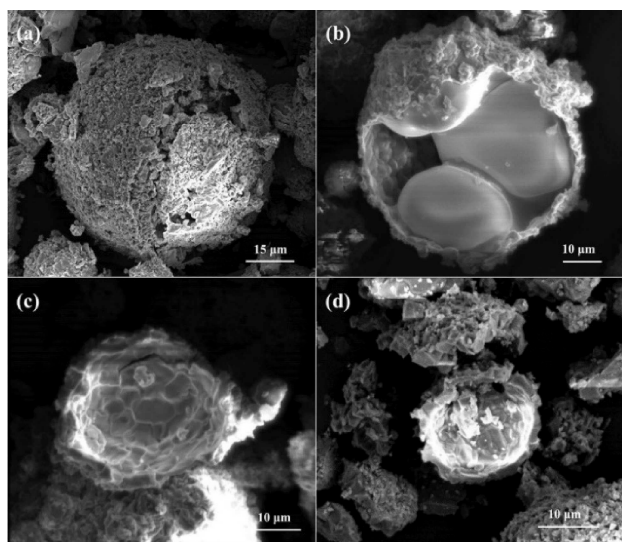


Figure 7. DSC curves of  $\text{ZrAl}_3$  under argon and oxygen.

exothermic peak under argon atmosphere. But there is a significantly exothermic peak under oxygen atmosphere near 960°C. This is consistent with previous Geßwein research and analysis on the oxidation kinetics of  $\text{ZrAl}_3$  particles [36]. We can conclude that the concentrated heat release of  $\text{ZrAl}_3$  in an oxygen atmosphere is responsible for the heat release of the  $\text{ZrAl}_3/\text{Al}$  composite fuels near 960°C.  $\text{ZrAl}_3$  has the characteristic of concentrated heat release at a specific temperature, which explains the phenomena in Figure 5. After melting of Al, the  $\text{ZrAl}_3$  gets exposed to oxygen ambience directly, and is oxidized prior to aluminum, which contributes to adequate contact of aluminum phase with oxygen and oxidation exotherm. Therefore, the temperature required to achieve the maximum weight increase ratio efficiency is significantly reduced with the increasing content of zirconium. When the content of zirconium is less than or equal to 30 wt.%, the content of  $\text{ZrAl}_3$  is low, the promotion effect on the oxidation exothermic of Al phase is not obvious, and the weight increase ratio of composite



**Figure 8.** SEM images of Al-30Zr composite fuels oxidized at 1300°C (a, b) and 1500°C (c, d).

fuels is not significant. But when the content of zirconium reaches 40 wt.% or more, the content of ZrAl<sub>3</sub> is enough high, the promotion effect on the oxidation exothermic of Al phase is obvious, and the weight increase ratio of composite fuels increases significantly.

### 3.3 Analysis of Oxidation Process

Based on above description and discussion, Al-30Zr composite fuels were used to study individually. The morphologies of Al-30Zr composite fuels oxidized at 1300°C and 1500°C are shown in Figure 8. It can be observed that the powder surface is substantially oxidized and the scales previously deposited on the surface of the Al-30Zr particles have disappeared. As shown in Figure 8(a) and Figure 8(b), there are a large number of cracks on the surface of the particle at 1300°C, part of the outer shell is ruptured, and the molten nucleuses inside the shell are exposed. It can be inferred that these nucleuses are formed by molten aluminum encased in ZrAl<sub>3</sub>. As shown in Figure 8(c) and Figure 8(d), the nucleuses disappear with only a broken empty shell left when the oxidation temperature reaches 1500°C. It is speculated that this empty shell must be made up of Al<sub>2</sub>O<sub>3</sub> and ZrO<sub>2</sub>, and at the point the sample has been completely oxidized. The XRD patterns of furnace-cooling products are shown in Figure 9. The oxidation product obtained at 1300°C is mainly composed of Al<sub>2</sub>O<sub>3</sub>, ZrO<sub>2</sub>, unreacted aluminum and ZrAl<sub>3</sub>. While the product obtained at 1500°C only consists of Al<sub>2</sub>O<sub>3</sub> and ZrO<sub>2</sub>, and all t-ZrO<sub>2</sub> turn into m-ZrO<sub>2</sub>. The results are consistent with the results of the earlier studies of [27,32] and also confirm the aforementioned speculation.

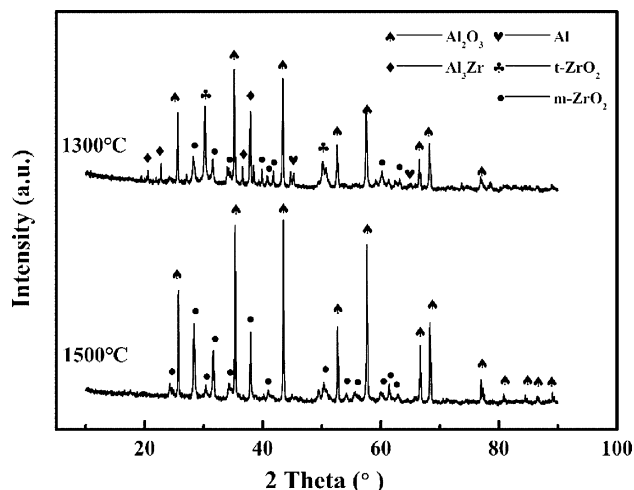


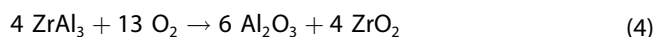
**Figure 9.** XRD patterns of oxidation products of the Al-30Zr composite fuels at different temperature.

Based on the above experimental results and analysis, a new oxidation mechanism of Al-30Zr composite fuels is proposed in Figure 10. According to the SEM image of the Al-30Zr composite fuels and the cross section of the particles (Figure 2b and Figure 3), we know that alumina and ZrAl<sub>3</sub> are present on the surface layer of the ZrAl<sub>3</sub>/Al composite fuels, and the contact between the two is not compact. Moreover, a large amount of ZrAl<sub>3</sub> exists inside the particle, a part of ZrAl<sub>3</sub> is connected to each other in the aluminum matrix, and the other part is independently distributed in the aluminum matrix. At the beginning, since the contact between the alumina and the ZrAl<sub>3</sub> on the surface layer of the ZrAl<sub>3</sub>/Al composite fuels is not compact, a small amount of oxygen penetrates through the surface, causing the aluminum inside the particle to be slowly oxidized. So that the initial reaction is driven by defects in alumina. The reaction is as follows:



As the temperature increases, the aluminum begins to melt and the ZrAl<sub>3</sub> inside the particle is wrapped up by liquid aluminum.

When reaching the temperature corresponding to the concentrated heat release of ZrAl<sub>3</sub> (about 960°C), the pure aluminum phase has completely melted to a liquid state. At the same time, the ZrAl<sub>3</sub> on the surface layer of the ZrAl<sub>3</sub>/Al composite fuels begin to undergo intense oxidation with oxygen. The oxidation process of ZrAl<sub>3</sub> is characterized by the non-selective oxidation of zirconium which forms ZrO<sub>2</sub> and Al<sub>2</sub>O<sub>3</sub> in oxygen atmosphere. The non-selective oxidation process of ZrAl<sub>3</sub> can be represented by the following equation:





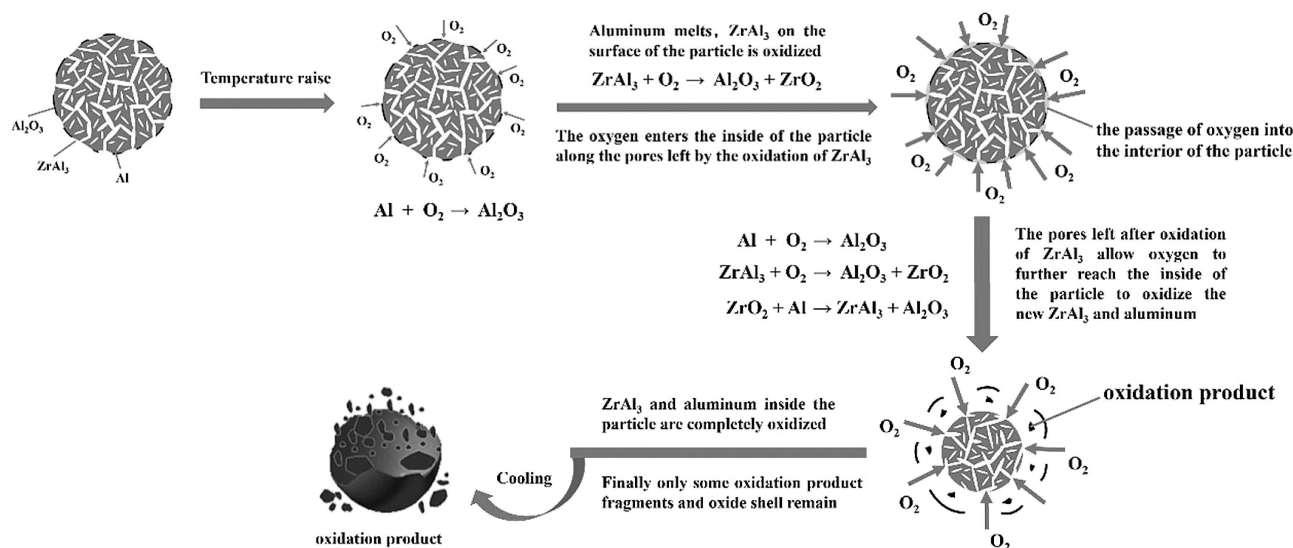
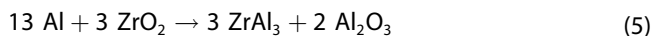


Figure 10. Scheme of oxidation process of the Al-30Zr composite fuels.

After this oxidation reaction,  $\text{ZrAl}_3$  on the surface layer of the  $\text{ZrAl}_3/\text{Al}$  composite fuels disappears, leaving a large amount of passages on the alumina shell. Oxygen enters the interior of the particle along the passages left after oxidation of  $\text{ZrAl}_3$ , undergoes a vigorous oxidation reaction with  $\text{ZrAl}_3$  and aluminum inside the particle, and releases a large amount of heat. At the same time, the reaction between aluminum and the dispersed oxidation products  $\text{ZrO}_2$  occurs [37], as is shown in equation (5). This reaction produces new  $\text{ZrAl}_3$  while releasing a lot of heat, and the new  $\text{ZrAl}_3$  is also able to participate in the reaction shown in equation (4) and release heat. The aluminum oxide film that aluminum inside the particle produces after oxidation limits the contact of oxygen with aluminum. However, there is a large amount of interconnected  $\text{ZrAl}_3$  inside the particle, and the passages left after oxidation of  $\text{ZrAl}_3$  allow oxygen to further reach the inside of the particle to oxidize the new  $\text{ZrAl}_3$  and aluminum.



In this way, oxygen can continuously enter the interior of the particle in a short time, so that  $\text{ZrAl}_3$  and aluminum inside the particle are completely oxidized, and finally only some oxidation product fragments and oxide shell remain, as shown in Figure 8(c) and Figure 8(d).

In a word, the content of zirconium plays an important role in the oxidation of  $\text{ZrAl}_3/\text{Al}$  composite fuels. The content of zirconium determines the amount of intermetallic compound  $\text{ZrAl}_3$  which plays an important role in the oxidation process of  $\text{ZrAl}_3/\text{Al}$  composite fuels. Thus, this study shows that the needle-shaped intermetallic compounds  $\text{ZrAl}_3$  embedded in the aluminum matrix obviously affects the oxidation of  $\text{ZrAl}_3/\text{Al}$  composite fuels.

### 3.4 Oxygen Bomb Experiment

In order to further study the exothermic properties of  $\text{ZrAl}_3/\text{Al}$  composite fuels, the samples with different zirconium content were tested under different pressures in the device (shown in Figure 1). The gravimetric and volumetric combustion enthalpies are used as the evaluation index of oxygen bomb experiment. Their relations are as follows:

$$H_v = \rho \times H_G \quad (6)$$

The results of density measured by spring dynamometer method are presented in Figure 11. Both the theoretical and the experimental density of  $\text{ZrAl}_3/\text{Al}$  composite fuels

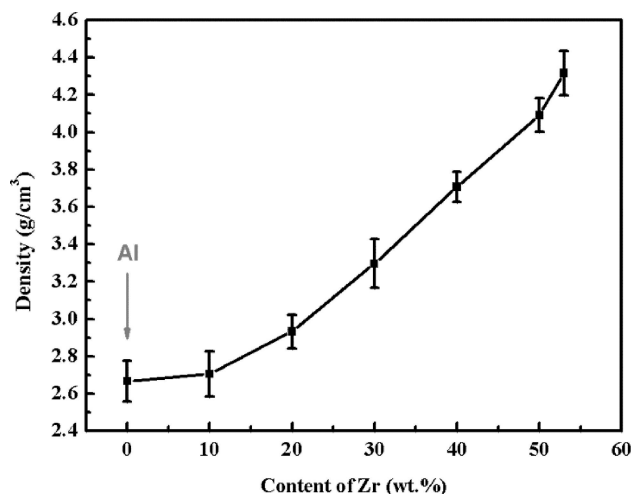


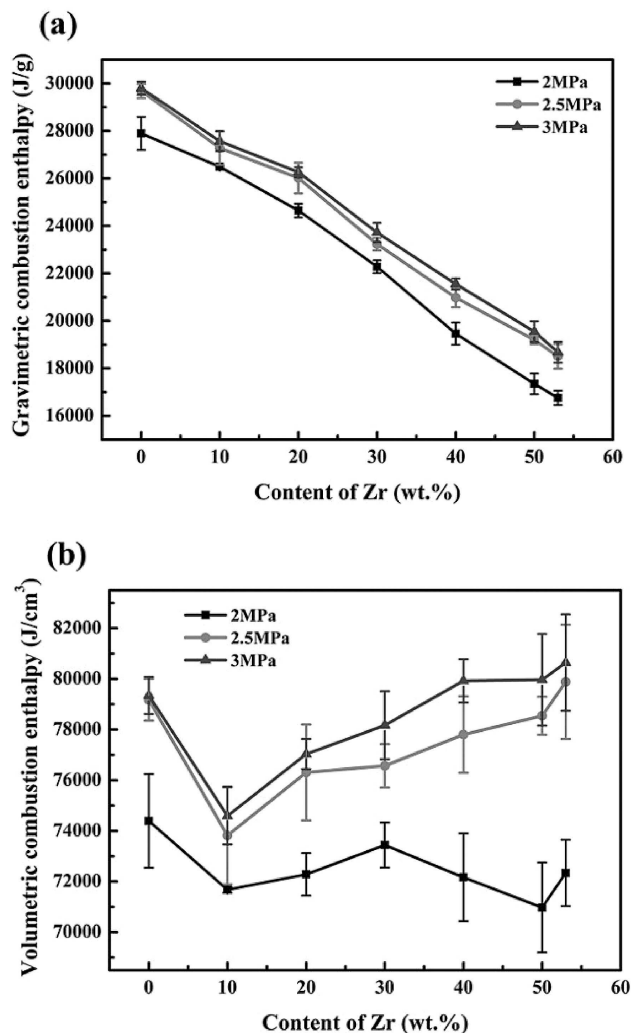
Figure 11. The bulk densities of Al-Zr alloys.

**Table 1.** The theoretical density and experimental density of  $\text{ZrAl}_3/\text{Al}$  composite fuels.

| Sample  | Al              | Al-10Zr         | Al-20Zr         | Al-30Zr         | Al-40Zr         | Al-50Zr         | Al-53Zr         |
|---|-----------------|-----------------|-----------------|-----------------|-----------------|-----------------|-----------------|
| theoretical density ( $\text{g}/\text{cm}^3$ )  | 2.7             | 2.87            | 3.06            | 3.27            | 3.52            | 3.82            | 3.91            |
| experimental density ( $\text{g}/\text{cm}^3$ ) | $2.67 \pm 0.11$ | $2.71 \pm 0.11$ | $2.93 \pm 0.09$ | $3.30 \pm 0.13$ | $3.71 \pm 0.08$ | $4.09 \pm 0.09$ | $4.32 \pm 0.12$ |

are shown in Table 1. It can be seen that the experimental density of pure Al is slightly lower than the theoretical density, because the bulk Al used in the experiment contains a small amount of impurities and the presence of an oxide layer on the surface. When zirconium is added, zirconium forms an intermetallic compound  $\text{ZrAl}_3$  with aluminum. Compared with the theoretical bulk density calculated by simple addition of pure Al and pure zirconium, the intermetallic compound  $\text{ZrAl}_3$  has a higher density due to atomic bonding. However, when the zirconium content is less than or equal to 20 wt.%, the intermetallic compound  $\text{ZrAl}_3$  content in the  $\text{ZrAl}_3/\text{Al}$  composite fuels is low, and the bulk Zr also contains a small amount of impurities, so the experimental density of the  $\text{ZrAl}_3/\text{Al}$  composite fuels is still slightly below the theoretical density. When the zirconium content reaches 30 wt.% or more, the  $\text{ZrAl}_3/\text{Al}$  composite fuels contain more intermetallic compounds  $\text{ZrAl}_3$ , and the experimental density of  $\text{ZrAl}_3/\text{Al}$  composite fuels exceeds the theoretical density.

At the same time, the pressure traces of the oxygen bomb experiment with different  $\text{ZrAl}_3/\text{Al}$  composite fuels are recorded synchronously. Pure aluminum powder is also measured in this test for comparison. The experimental result of the combustion enthalpies of each  $\text{ZrAl}_3/\text{Al}$  composite fuels is given in Figure 12. As can be seen from Figure 12(a), with the increase of Zr content, the  $H_G$  shows a linear downward trend. Meanwhile, the  $H_G$  increases with the increase of pressure. These results accord with the fact that the gravimetric combustion enthalpy of aluminum powder is higher than that of zirconium powder and higher pressure promotes the composite fuels burning more sufficiently. The  $H_V$  of different  $\text{ZrAl}_3/\text{Al}$  composite fuels are shown in Figure 12(b). With the increase of zirconium content, the change trend of weight and volume combustion heat is different, which is attributed to the increase of density of  $\text{ZrAl}_3/\text{Al}$  composite fuels with the increase of zirconium content. It's obviously that with the increasing of Zr content, there is a general upward trend in the  $H_V$  when the pressure is higher than 2.5 MPa and the Zr content exceeds 10 wt.%. At the pressure of 3 MPa, the  $H_V$  of  $\text{ZrAl}_3/\text{Al}$  composite fuels with higher content of Zr is more than that of the pure aluminum powders. The maximum  $H_V$  of  $\text{ZrAl}_3/\text{Al}$  composite fuels is as high as  $80642.9 \text{ J}/\text{cm}^3$ . However, the  $H_V$  curve presents the different change that the  $H_V$  first ascends and then descends when pressure is less than 2.5 MPa, which can be ascribed to incomplete combustion of  $\text{ZrAl}_3/\text{Al}$  composite fuels. Comparing with the theoretical values (shown in Table 2), the values of  $H_G$  and  $H_V$  are slightly lower, which may be attributed to experiment error

**Figure 12.** Gravimetric combustion enthalpy and volumetric combustion enthalpy of  $\text{Al}_3\text{Zr}/\text{Al}$  composite fuels.

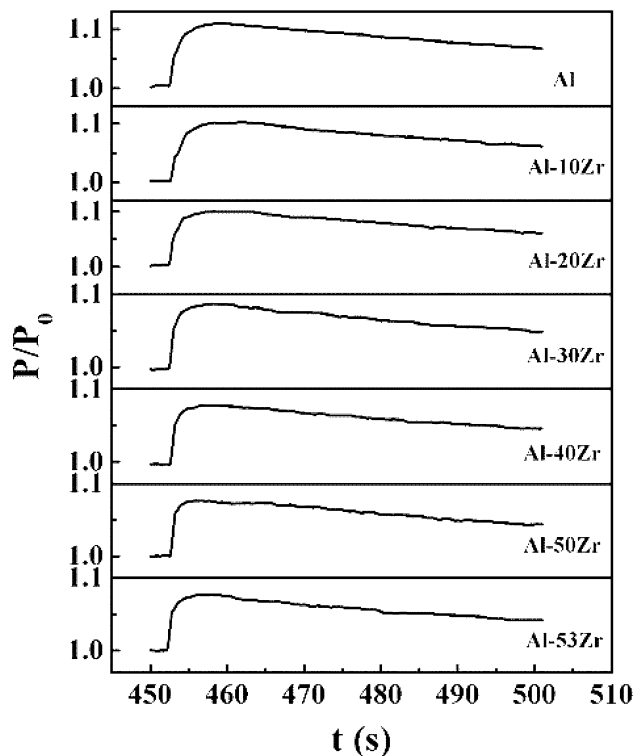
and impurity content, etc. Therefore, under high pressure, the volumetric combustion energy of the  $\text{ZrAl}_3/\text{Al}$  composite fuels can exceed that of aluminum powder, and the  $\text{ZrAl}_3/\text{Al}$  composite fuels exhibits excellent exothermic performance.

Using a modified oxygen bomb combustion apparatus, the gas pressure of  $\text{ZrAl}_3/\text{Al}$  composite fuels in oxygen bomb were investigated. Figure 13 shows a series of the pressure traces of  $\text{ZrAl}_3/\text{Al}$  composite fuels with different zirconium contents measured in the oxygen bomb experiments at 3 MPa. All samples shown in Figure 13 were ig-

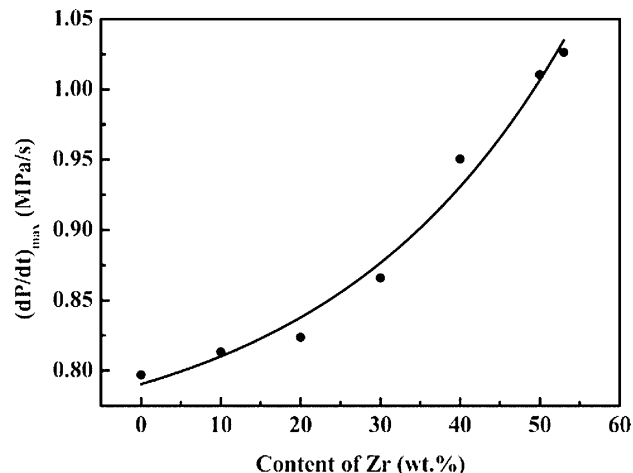


**Table 2.** The combustion enthalpies of  $\text{ZrAl}_3/\text{Al}$  composite fuels at 3 MPa, 2.5 MPa and 2 MPa.

| Sample  | theoretical value      |                                       | 3 MPa                 |                                      | 2.5 MPa               |                                      | 2 MPa                 |                                      |
|---------|------------------------|---------------------------------------|-----------------------|--------------------------------------|-----------------------|--------------------------------------|-----------------------|--------------------------------------|
|         | $H_{\text{Gt}}$ (kJ/g) | $H_{\text{Vt}}$ (kJ/cm <sup>3</sup> ) | $H_{\text{G}}$ (kJ/g) | $H_{\text{V}}$ (kJ/cm <sup>3</sup> ) | $H_{\text{G}}$ (kJ/g) | $H_{\text{V}}$ (kJ/cm <sup>3</sup> ) | $H_{\text{G}}$ (kJ/g) | $H_{\text{V}}$ (kJ/cm <sup>3</sup> ) |
| Al      | 30.54                  | 82.46                                 | $29.80 \pm 0.28$      | $79.35 \pm 0.74$                     | $29.69 \pm 0.30$      | $79.18 \pm 0.82$                     | $27.89 \pm 0.69$      | $74.39 \pm 1.85$                     |
| Al-10Zr | 28.69                  | 82.25                                 | $27.57 \pm 0.42$      | $74.59 \pm 1.13$                     | $27.28 \pm 0.71$      | $73.82 \pm 1.93$                     | $26.49 \pm 0.44$      | $71.68 \pm 0.12$                     |
| Al-20Zr | 26.84                  | 82.04                                 | $26.26 \pm 0.20$      | $77.03 \pm 0.60$                     | $26.02 \pm 0.64$      | $76.30 \pm 1.89$                     | $24.64 \pm 0.29$      | $72.28 \pm 0.84$                     |
| Al-30Zr | 24.99                  | 81.78                                 | $23.72 \pm 0.41$      | $78.17 \pm 1.34$                     | $23.23 \pm 0.26$      | $76.57 \pm 0.86$                     | $22.28 \pm 0.27$      | $73.44 \pm 0.89$                     |
| Al-40Zr | 23.14                  | 81.51                                 | $21.55 \pm 0.23$      | $79.92 \pm 0.85$                     | $20.98 \pm 0.41$      | $77.80 \pm 1.51$                     | $19.46 \pm 0.47$      | $72.17 \pm 1.73$                     |
| Al-50Zr | 21.29                  | 81.16                                 | $19.55 \pm 0.44$      | $79.97 \pm 1.81$                     | $19.20 \pm 0.18$      | $78.54 \pm 0.75$                     | $17.35 \pm 0.43$      | $70.97 \pm 1.78$                     |
| Al-53Zr | 20.73                  | 81.05                                 | $18.68 \pm 0.44$      | $80.64 \pm 1.90$                     | $18.50 \pm 0.52$      | $79.88 \pm 2.25$                     | $16.76 \pm 0.30$      | $72.34 \pm 1.31$                     |

**Figure 13.** The P-t curves of  $\text{ZrAl}_3/\text{Al}$  composite fuels under 3 MPa.

nited at  $t=425$  s. At the moment of ignition, the pressure in the bomb suddenly increases to the maximum value  $P_{\text{max}}$  and then slowly decreases as the temperature decreases. The corresponding data are all listed in Table 3. Figure 14 shows the corresponding graph of maximum pressurization rate  $(dP/dt)_{\text{max}}$ , which characterizes the maximum flame propagation rate and higher energy releasing rates. As shown in Figure 14, the fitting curve of pressurization rate

**Figure 14.** The maximum pressurization rate as a function of Zr content.

with different  $\text{ZrAl}_3/\text{Al}$  composite fuels under 3 MPa is exponential. It can be seen from Figure 14 that as the Zr content increases, the maximum pressurization rate of the  $\text{ZrAl}_3/\text{Al}$  composite fuels increases, the reaction becomes faster. Moreover, the comparison shows that Al-53Zr composite fuels have the maximum pressurization rate in the experimentally prepared series of composite fuels.

Combustion products of Al-30Zr after the above combustion experiment were collected and analyzed by XRD. As shown in Figure 15, the XRD pattern shows that  $\text{Al}_2\text{O}_3$ ,  $\text{t-ZrO}_2$  and  $\text{m-ZrO}_2$  are main phases in the combustion products at 3 MPa. Unreacted Al and  $\text{ZrAl}_3$  are absent from the diffraction pattern. The result shows that  $\text{ZrAl}_3/\text{Al}$  composite fuels has combusted completely.

Based on the condition of complete combustion, the effect of pressure on thermal properties of the  $\text{ZrAl}_3/\text{Al}$  com-

**Table 3.** The summary of experimental results of oxygen bomb.

| Sample                         | Al       | Al-10Zr  | Al-20Zr  | Al-30Zr  | Al-40Zr  | Al-50Zr  | Al-53Zr  |
|--------------------------------|----------|----------|----------|----------|----------|----------|----------|
| $P_{\text{max}}$ (MPa)         | 3.239721 | 3.239721 | 3.218543 | 3.218543 | 3.212190 | 3.135950 | 3.157128 |
| $P_{\text{max}}/P_0$           | 1.11275  | 1.10232  | 1.10067  | 1.08728  | 1.08281  | 1.07946  | 1.07966  |
| $(dP/dt)_{\text{max}}$ (MPa/s) | 0.796973 | 0.813381 | 0.82373  | 0.865978 | 0.950465 | 1.010491 | 1.026324 |

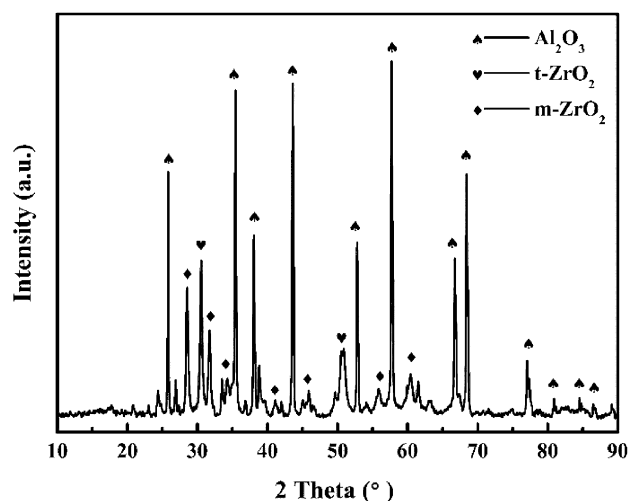


**Figure 15.** XRD patterns of combustion products of the Al-30Zr composite fuels under 3 MPa.

posite fuels is studied. The gas temperature inside the oxygen bomb at the maximum pressure is calculated according to the Van der Waals' gas state equation of real gas shown in equation (7). The meanings of all coefficients and variables are listed after the text. In this formula,  $a$  is  $0.1378 \text{ L}^2 \cdot \text{Mpa} \cdot \text{mol}^{-2}$  and  $b$  is  $0.031 \text{ L} \cdot \text{mol}^{-1}$ . Some assumptions are made as follows: a) The gas in oxygen bomb is pure oxygen. b) The sample has been burnt out at the maximum pressure.

$$\left(p + \frac{an^2}{V^2}\right)(V - nb) = nRT \quad (7)$$

The fitting curves of the average gas temperature in the oxygen bomb with different oxygen pressure are shown in Figure 16. As can be seen from Figure 16, the temperature at the maximum gas pressure decreases linearly with the increase of Zr content, which is consistent with the results of Figure 12(a). Combined with the thermal analysis and oxygen bomb test results, it can be reasonably concluded that with the increase of zirconium content, the gravimetric combustion enthalpy decreases and the degree of oxidation increases. Moreover, under the same oxygen pressure, as the Zr content increases, the amount of heat released by the oxidation of the composite fuels and the amount of oxygen consumed decrease, which will result in a decrease in the average temperature of the gas in the oxygen bomb. On the other hand, the average temperature of the gas increases as the oxygen pressure decreases. We estimate that this is related to the lower residual oxygen content in a fixed volume of oxygen bombs after combustion of the composite fuels at low oxygen pressure. In general, we can change the average gas temperature at the maximum gas pressure and improve the combustion efficiency by regulating the oxygen partial pressure and content of Zr.

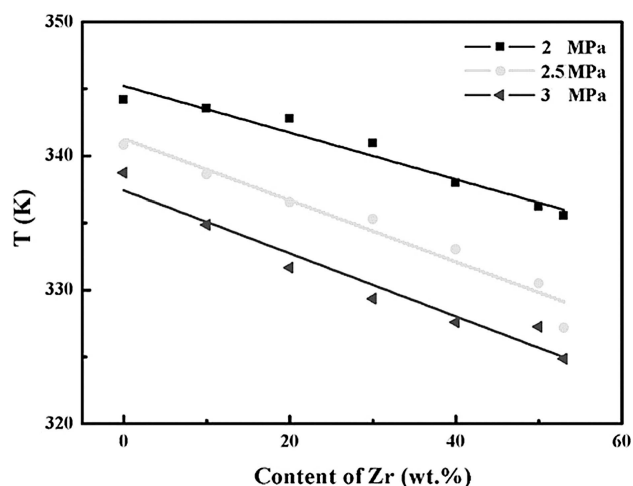


**Figure 16.** The average gas temperature at the maximum gas pressure in the oxygen bomb as a function of Zr content.

## 4 Conclusions

A series of  $\text{ZrAl}_3/\text{Al}$  composite fuels with the Zr content ranging from 10 to 53 wt.% have been prepared successfully. The experimental results are summarized as follows:

The  $\text{ZrAl}_3/\text{Al}$  composite fuels mainly consists of Al phase and  $\text{ZrAl}_3$  phase. With the increase of Zr content, the exothermic temperature of  $\text{ZrAl}_3/\text{Al}$  composite fuels decreases and the weight increase ratio increases (all more than that of pure Al). A special structure forming in the interior of a particle may promote the oxidation of  $\text{ZrAl}_3/\text{Al}$  composite fuels. Moreover, the non-selective oxidation of  $\text{ZrAl}_3$  plays a key role in oxidation process. Oxygen bomb experiments show that both oxygen pressure and Zr content have a significant effect on the combustion enthalpies of the composite fuels. the Al-53Zr composite fuel has the maximum pressure propagation rate  $(dP/dt)_{\text{max}}$  in the prepared series of composite fuels. In addition,  $\text{ZrAl}_3/\text{Al}$  composite fuels can be completely burned under high oxygen pressure. The maximum value of the volumetric combustion enthalpy of  $\text{ZrAl}_3/\text{Al}$  composite fuels is  $80642.9 \text{ J/cm}^3$  when Zr content is 53 wt.% and the oxygen pressure is 3 MPa. In summary, compared with pure aluminum powder,  $\text{ZrAl}_3/\text{Al}$  composite fuels have higher density, lower oxidation peak temperature, greater oxidation weight increase ratio, faster oxidation rate and more complete combustion without significantly reducing oxidation heat release. Thus,  $\text{ZrAl}_3/\text{Al}$  composite fuels could be considered as a very promising energetic additive in the field of new-energetic material.

## Symbols and Abbreviations

|       |                                 |
|-------|---------------------------------|
| F     | buoyancy                        |
| G     | gravity                         |
| $T_0$ | pulling force immersed in water |

|                  |                                 |
|------------------|---------------------------------|
| $\rho$           | bulk density of alloys          |
| $\rho_0$         | density of water                |
| $g$              | gravitational acceleration      |
| $m$              | mass of alloys                  |
| $V$              | displacement volume of alloys   |
| $H_v$            | volumetric combustion enthalpy  |
| $H_G$            | gravimetric combustion enthalpy |
| $P_{\max}$       | the maximum pressure            |
| $(dP/dt)_{\max}$ | the maximum pressurization rate |
| $V_0$            | volume of oxygen bomb           |
| $n$              | amount of substance of oxygen   |
| $a$              | Van Der Waals constant          |
| $b$              | Van Der Waals constant          |
| $R$              | gas constant                    |
| $T$              | temperature                     |

## Subscripts

t theoretical value

## Acknowledgements

The authors gratefully acknowledge the financial support from the National Natural Science Foundation of China (51871106) and "NSAF" joint fund (U1530127) set up by the National Natural Science Foundation and China Academy of Engineering Physics jointly. To express my gratitude for analyzing and testing of the analysis and test center in Huazhong University of Science and Technology.

## References

- [1] A. Gany, D. W. Netzer, Fuel performance evaluation for the solid-fueled ramjet, *Int. J. Turbo Jet. Eng.* **1985**, 2, 157–168.
- [2] B. Palaszewski, R. Powell, Launch vehicle performance using metallized propellants, *J. Propul. Power* **1994**, 10, 828–833.
- [3] F. Maggi, S. Dossi, C. Paravan, L. T. DeLuca, M. Liljedahl, Activated aluminum powders for space propulsion, *Powder Technol.* **2015**, 270, 46–52.
- [4] S. M. Umbrajkar, M. Schoenitz, S. R. Jones, E. L. Dreizin, Effect of temperature on synthesis and properties of aluminum-magnesium mechanical alloys, *J. Alloys Compd.* **2005**, 402, 70–77.
- [5] J. T. Moore, S. R. Turns, R. A. Yetter, Combustion of lithium-aluminum alloys, *Combust. Sci. Technol.* **2015**, 177, 627–669.
- [6] W. R. Osório, J. E. Spinelli, C. R. Afonso, L. C. Peixoto, A. Garcia, Electrochemical corrosion behavior of gas atomized Al–Ni alloy powders, *Electrochim. Acta* **2012**, 69, 371–378.
- [7] Y. L. Shoshin, E. L. Dreizin, Particle combustion rates for mechanically alloyed Al–Ti and aluminum powders burning in air, *Combust. Flame* **2006**, 145, 714–722.
- [8] Y. Aly, M. Schoenitz, E. L. Dreizin, Preparation, ignition and combustion of mechanically alloyed Al–Mg powders with customized particle sizes, *Combust. Flame* **2013**, 160, 835–842.
- [9] Y. Aly, E. L. Dreizin, Ignition and combustion of Al–Mg alloy powders prepared by different techniques, *Combust. Flame* **2015**, 162, 1440–1447.
- [10] Y. L. Shoshin, E. L. Dreizin, Particle combustion rates for mechanically alloyed Al–Ti and aluminum powders burning in air, *Combust. Flame* **2016**, 145, 714–722.
- [11] A. Llyin, A. Gromov, V. An, F. Faubert, C. D. Lzarra, A. Espagnacq, L. Brunet, Characterization of aluminum powders. I: parameters of reactivity of aluminum powders, *Propellants Explos. Pyrotech.* **2012**, 27, 361–364.
- [12] V. A. Ermakov, A. A. Razdobreev, A. I. Skorik, V. V. Pozdeev, S. S. Smolyakov, Temperature of aluminum particles at the time of ignition and combustion, *Combust. Explos. Shock* **1982**, 18, 256–257.
- [13] E. L. Dreizin, Experimental study of stages in aluminum particle combustion in air, *Combust. Flame* **1996**, 105, 541–556.
- [14] S. Hasani, M. Panjepour, M. Shamanian, The oxidation mechanism of pure aluminum powder particles, *Oxid. Met.* **2012**, 78, 179–195.
- [15] R. Friedman, A. Maček, Ignition and combustion of aluminum particles in hot ambient gases, *Combust. Flame* **1962**, 6, 9–19.
- [16] B. K. Athawale, S. N. Asthana, H. Singh, Metallised Fuel-rich Propellants for Solid Rocket Ramjet: A Review, *Defence Sci. J.* **2013**, 44, 269–278.
- [17] H. Oshima, M. Tanabe, T. Kuwahara, Ignition Characteristics of Zr with Micro Ducted Rockets, *42nd AIAA/ASME/SAE/ASEE Joint Propulsion Conference & Exhibit, Sacramento, California, AIAA*. 9–12 July **2006**, 2006–5248.
- [18] I. M. Procinsky, C. A. Mchale, Nozzleless Boosters for Integral-Rocket-Ramjet Missile Systems, *J. Spacecr. Rockets* **1981**, 18, 193–199.
- [19] T. Suzuki, T. Odawara, K. Kunitou, M. Tanabe, T. Kuwahara, Combustion and ignition characteristics of Zr in solid fuel of ducted rockets, *Bull. Exp. Biol. Med.* **2004**, 94, 853–856.
- [20] A. A. Gromov, Y. I. Pautova, A. M. Lider, A. G. Korotkikh, U. Teipel, E. V. Chaplina, T. I. Sigfusson, Interaction of powdery Al, Zr and Ti with atmospheric nitrogen and subsequent nitride formation under the metal powder combustion in air, *Powder Technol.* **2011**, 214, 229–236.
- [21] E. Malikova, J. Pautova, A. Gromov, K. Monogarov, K. Larionov, U. Teipel, On the mechanism of zirconium nitride formation by zirconium, zirconia and yttria burning in air, *J. Solid State Chem.* **2015**, 230, 199–208.
- [22] B. S. Min, H. S. Hyun, Study on Combustion Characteristics and Performance of HTPB/AP Propellants Containing Zirconium, *J. Propul. Power* **2015**, 28, 211–213.
- [23] M. Song, M. Zhang, B. Huang, S. Zhang, J. Li, Reaction Synthesis of  $ZrAl_3$ , Intermetallic Compound and Its Nucleation Behavior, *Rare Met.* **2008**, 37, 1570–1574.
- [24] M. S. Song, M. W. Ran, Only Formation of  $ZrAl_3$  Phase Obtained by Self-Propagating Reaction from Zr–Al Elemental Powders, *Adv. Mater.* **2011**, 239–242, 2805–2808.
- [25] U. Anselmi-Tamburini, G. Spinolo, G. Flor, Z. A. Munir, Combustion synthesis of Zr–Al intermetallic compounds, *J. Alloys Compd.* **1997**, 247, 190–194.
- [26] M. Paljević, Change of oxidation kinetics in the Zr–Al system, *J. Less-Common Met.* **1990**, 157, 289–293.
- [27] M. Paljević, Non-Selective Oxidation of  $ZrAl_3$ , *Less-Common Met.* **1991**, 175, 289–294.
- [28] M. Vohra, J. Winokur, K. R. Overdeep, P. Marcello, T. P. Weihs, O. M. Knio, Development of a reduced model of formation reactions in Zr–Al nanolaminates, *J. Appl. Phys.* **2014**, 116, 288–295.
- [29] K. R. Overdeep, K. J. T. Livi, D. J. Allen, N. G. Glumac, T. P. Weihs, Using magnesium to maximize heat generated by reactive Al/Zr nanolaminates, *Combust. Flame* **2015**, 162, 2855–2864.
- [30] E. R. Wainwright, T. A. Schmauss, S. V. Lakshman, K. R. Overdeep, T. P. Weihs, Observations during Al:Zr composite particle combustion in varied gas environments, *Combust. Flame* **2018**, 196, 487–499.

- [31] S. V. Lakshman, J. D. Gibbins, E. R. Wainwright, T. P. Weihs, The effect of chemical composition and milling conditions on composite microstructure and ignition thresholds of  $\text{AlZr}$  ball milled powders, *Powder Technol.* **2019**, 343, 87–94.
- [32] H. Zou, L. Li, S. Cai, Effect of Magnesium-Rich Phase on Oxidation Properties of Atomized Aluminum–Magnesium Powders, *J. Propul. Power* **2015**, 32, 1–6.
- [33] L. Li, H. Zou, S. Cai, Thermal behaviour of gas atomised  $\text{Al-20Mg-2Zr}$  alloy powder, *Mater. Sci. Technol.* **2016**, 32, 32–37.
- [34] H. Fu, H. Zou, S. Z. Cai, The role of microstructure refinement in improving the thermal behavior of gas atomized  $\text{Al-Eu}$  alloy powder, *Adv. Powder Technol.* **2016**, 27, 1898–1904.
- [35] M. Schoenitz, E. L. Dreizin, E. Shtessel, Constant Volume Explosions of Aerosols of Metallic Mechanical Alloys and Powder Blends, *J. Propul. Power* **2003**, 19, 405–412.
- [36] H. Geßwein, J. R. Binder, Thermokinetic study of the oxidation of  $\text{ZrAl}_3$  powders, *Thermochim. Acta* **2006**, 444, 6–12.
- [37] A. Mandal, K. Das, S. Das, Characterization of microstructure and properties of  $\text{Al-Al}_3\text{Zr-Al}_2\text{O}_3$  composite, *Bull. Mater. Sci.* **2016**, 39, 1–12.

Manuscript received: January 10, 2019  
Revised manuscript received: March 30, 2019  
Version of record online: July 16, 2019